Premature endocycling of *Drosophila* follicle cells causes pleiotropic defects in oogenesis

Hunter C. Herriage[1] and Brian R. Calvi[1,2,3,4]

1: Department of Biology, Indiana University, Bloomington, IN 47405

2: Melvin and Bren Simon Cancer Center, Indianapolis, IN

3: Indiana University School of Medicine, Bloomington, IN

4: Corresponding author, bcalvi@indiana.edu

Keywords: endocycling, border cells, polyploidy, oogenesis, epithelium, *Drosophila*

16 **Summary Statement**

17 A premature switch to polyploid endocycles in *Drosophila* ovarian follicle cells caused
18 pleiotropic defects in oogenesis and compromised female fertility, revealing new ways in which
19 unscheduled endocycles cause developmental defects.

20

Abstract

Endocycling cells grow and repeatedly duplicate their genome without dividing. Cells switch from mitotic cycles to endocycles in response to developmental signals during the growth of specific tissues in a wide range of organisms. The purpose of switching to endocycles, however, remains unclear in many tissues. Additionally, cells can switch to endocycles in response to conditional signals, which can have beneficial or pathological effects on tissues. However, the impact of these unscheduled endocycles on development is underexplored. Here, we use *Drosophila* ovarian somatic follicle cells as a model to examine the impact of unscheduled endocycles on tissue growth and function. Follicle cells normally switch to endocycles at mid-oogenesis. Inducing follicle cells to prematurely switch to endocycles resulted in lethality of the resulting embryos. Analysis of ovaries with premature follicle cell endocycles revealed aberrant follicular epithelial structure and pleiotropic defects in oocyte growth, developmental gene amplification, and the migration of a special set of follicle cells known as border cells. Overall, these findings reveal how unscheduled endocycles can disrupt tissue growth and function to cause aberrant development.

Introduction

Many tissues grow via a variant cell cycle known as the endocycle. Endocycles are characterized by alternating G and S phases without mitotic division, resulting in the growth of large polyploid cells (Calvi 2013; Ovrebo and Edgar 2018; Fox *et al.* 2020). A regulated switch from mitotic cycles to endocycles is part of the normal developmental growth programs of specific tissues across *Eukarya* (Ovrebo and Edgar 2018; Fox *et al.* 2020). In contrast, cells can also switch to unscheduled endocycles in response to stress and other conditional signals (Hassel *et al.* 2014; Rotelli *et al.* 2019; Bailey *et al.* 2021; Besen-McNally *et al.* 2021). These induced endocycling cells can be beneficial for wound healing and regeneration, but they can also have pathological effects, including the promotion of genome instability and cancer (Shu *et al.* 2018; Stormo and Fox 2019; Bailey *et al.* 2021; Almeida Machado Costa *et al.* 2022; Pienta *et al.* 2022; Herriage *et al.* 2023). Much remains unknown, however, about how unscheduled endocycling affects tissue structure and function.

In this study we used the somatic follicle cells of the *Drosophila* ovary as a model to evaluate the effects of unscheduled endocycles on tissue function. A *Drosophila* ovary consists of ~16 ovarioles, each composed of one germarium stem cell compartment followed by an “assembly line” of progressively developing egg chambers in 14 stages of oogenesis (Fig. 1A) (King 1970; Duhart *et al.* 2017). These developing egg chambers contain the germline (15 endocycling nurse cells and one oocyte) ensheathed by an epithelium of somatic follicle cells (Fig. 1A) (King 1970; Jia *et al.* 2015; Duhart *et al.* 2017). Follicle cells originate from a population of two to four somatic stem cells in the germarium and proliferate mitotically over the course of three days until stage 6 of oogenesis (Margolis and Spradling 1995; Sun and Deng 2007; Fadiga and Nystul 2019). In response to Notch signaling from the germline at stages 6 / 7, follicle cells switch to the endocycle and subsequently complete three genome duplications over the next ~24 hours (Fig. 1A) (Spradling 1993; Calvi *et al.* 1998; Deng *et al.* 2001; Lopez-Schier and St Johnston 2001). After achieving a DNA copy number (C) of 16C, follicle cells asynchronously arrest endocycles at different times during late stage 9 (Calvi *et al.* 1998). Follicle cells then synchronously initiate a specialized DNA rereplication program in stage 10B that selectively amplifies the DNA copy number of eggshell (chorion) protein genes, a process known as chorion gene amplification (Fig. 1A) (Spradling and Mahowald 1980; Calvi *et al.* 1998). Disruption of this developmental gene amplification causes thin eggshells and

68 embryonic lethality (Spradling and Mahowald 1980; Calvi 2006; Hua and Orr-Weaver 2017). It
69 has been shown that the endocycle to amplification transition requires the downregulation of
70 Notch signaling and the modification of several transcription factor and cell cycle protein
71 activities (Calvi *et al.* 1998; Royzman *et al.* 1999; Bosco *et al.* 2001; Cayirlioglu *et al.* 2001;
72 Beall *et al.* 2002; Beall *et al.* 2004; Calvi 2006; Sun *et al.* 2008; Huang *et al.* 2013; Jia *et al.*
73 2015). Much remains unknown, however, about the molecular mechanism of endocycle arrest
74 and the selective activation of amplification origins at precise times of oogenesis. Follicle cells
75 also support egg growth by mediating transport of yolk proteins into the oocyte and participate
76 in the axial patterning of the egg and embryo (Brennan *et al.* 1982; Raikhel and Dhadialla
77 1992; Duhart *et al.* 2017; Merkle *et al.* 2020). While it is known that follicle cells have these
78 important roles in oogenesis, it remains unclear what biological function is served by the
79 endocycle switch occurring specifically at stage 6. In this study, we find that inducing
80 endocycles to switch to endocycles earlier than stage 6 has severe negative consequences for
81 oogenesis and female fertility, with broader impacts on understanding how unscheduled
82 endocycles may contribute to human disease.
83
84 **Results**
85 Premature endocycles cause structural defects in the follicular epithelium
86 To address whether a switch to follicle cell endocycles before stage 6 would affect
87 oogenesis, we induced premature endocycling by expressing the protein Roughex (Rux), a
88 repressor of Cyclin A / CDK1 activity and mitotic entry that has been shown to induce
89 endocycles in other tissues (Thomas *et al.* 1994; Sprenger *et al.* 1997; Avedisov *et al.* 2000;
90 Vidwans *et al.* 2002). We used a *tj-GAL4* transgene to induce expression of a *UAS-Rux*
91 transgene in all ovarian somatic cells, and a temperature-sensitive GAL80^{ts} repressor of GAL4
92 to control the timing of expression (Brand and Perrimon 1993; McGuire *et al.* 2004; Weaver *et*
93 *al.* 2020). The *tj-GAL4 tub-GAL80ts / UAS-Rux* experimental and *tj-GAL4 tub-GAL80^{ts} /* +
94 control animals were raised at 18°C to repress GAL4 activity during development. Adult flies
95 were then shifted to 29°C to induce *UAS-Rux* expression and ovaries were examined one and
96 two days thereafter. Given that expression of *Cyclin A* is repressed in endocycling follicle cells
97 after stage 6, it was expected Rux would only impact follicle cell mitotic cycles (Sun and Deng
98 2005). Consistent with this, within one day after *UAS-Rux* expression, stage 1-6 follicle cells
99 ceased labeling for the mitotic marker phosphorylated Histone H3 (pH3) but continued to

100 incorporate the nucleotide analog 5-ethynyl 2′-deoxyuridine (EdU), indicating that they had
101 switched to G / S endocycles (Fig. S1A-F).
102 To determine the effects of induced endocycling on early stages of oogenesis, we
103 examined the structure of the follicular epithelium. To do this, we immunolabeled the cell
104 periphery with antibodies against the membrane-associated cell-cell junction protein E-
105 cadherin and stained nuclei with DAPI (Tepass *et al.* 1996; Uemura *et al.* 1996; Oda *et al.*
106 1997; Godt and Tepass 1998). After two days at 29°C, follicle cells in control ovaries had the
107 normal uniform, cuboidal structure and E-cadherin labeling that was greatest on their apical
108 surface adjacent to the germline (Fig. 1B-B″) (Godt and Tepass 1998; Gonzalez-Reyes and St
109 Johnston 1998). In contrast, after two days of Rux expression, follicle cells were all larger with
110 wide variations in their size and shape (Fig. 1C-C″). Some follicle cells had highly irregular
111 shapes, with different parts of the cell having unequal thicknesses in the apical-basal axis, and
112 many with highly irregular E-cadherin labeling (Fig. 1C-C″). In confocal sections through the
113 middle of egg chambers, the interface between the follicular epithelium and germline appeared
114 wavy instead of the normal smooth circular interface, indicating global deformations of tissue
115 morphology (Fig. 1B′, C′).
116 Measurement of the DNA content and diameter of the follicle cells on the surface of
117 stage 4 / 5 egg chambers revealed that premature endocycling follicle cells were polyploid and
118 larger than mitotic cycling control follicle cells consistent with their growth through hypertrophy
119 (Fig. 1D-G). These measurements also showed that these premature endocycling cells have a
120 large variance in their size and shape (Fig. 1D-G). Immunolabeling for the cell junction protein
121 beta-catenin, which is known as Armadillo (Arm) in *Drosophila,* or the membrane-associated
122 protein Discs large 1 (Dlg1), also supported the conclusion that premature endocycles caused
123 aberrant cell and epithelial structure and irregular cell-cell junctions (Figs. S2 and S3).
124 Although cell morphology was highly aberrant, Dlg1 had an overall normal basolateral
125 localization, suggesting that there was not a severe disruption of cell polarity (Fig. S3) (Woods
126 *et al.* 1996; Khoury and Bilder 2020). Induction of premature endocycles by RNAi knockdown
127 of *cyclin A* or over-expression of the Cdh1 ubiquitin ligase, *fizzy-related* (*fzr*) also resulted in
128 aberrant cell and epithelial structure, indicating that these effects are not specific to *Rux*
129 overexpression (Fig S4). Overall, these data indicate that induction of unscheduled follicle cell
130 endocycles earlier in oogenesis results in extremely aberrant cell and epithelial structure.
131

132 <u>Premature endocycling increases follicle cell terminal ploidy and causes cell cycle defects in</u>
133 <u>later stages of oogenesis</u>
134 We next asked what effect premature endocycles would have on follicle cells and egg
135 chambers as they matured to later stages of oogenesis (Fig. 2A). Two days after a shift to
136 29°C, control stage 10B egg chambers had the normal ~641 follicle cells and DNA content of
137 ~16C (Fig. 2B-B′, D, E) (Calvi *et al.* 1998; Sun and Deng 2007). In contrast, the induction of
138 premature endocycles two days earlier in *UAS-Rux* expressing ovaries resulted in stage 10B
139 egg chambers that had four-fold fewer follicle cells (~179) with a nearly a four-fold increase in
140 average DNA content (mean ploidy ~56 C) (Fig. 2C-E). These stage 10B follicle cells were
141 larger than normal, consistent with the known scaling of cell size with DNA ploidy (Fig. 2B′, C′)
142 (Tepass *et al.* 1996; Uemura *et al.* 1996; Cadart and Heald 2022). The four-fold decrease in
143 cell number together with a four-fold increase in DNA content suggested that Rux-expressing
144 follicle cells had skipped two mitotic divisions and instead underwent two extra endocycle
145 genome doublings. This conclusion is consistent with the known rate of oogenesis at 29°C
146 (Gandara and Drummond-Barbosa 2022). These stage 10B egg chambers would have been in
147 approximately stage 4 / 5 two days earlier at the time of temperature shift (Gandara and
148 Drummond-Barbosa 2022) (Fig. 2A). Normally, follicle cells in a stage 4 / 5 egg chamber
149 undergo an average of two mitotic divisions over one day as it matures to stage 6 / 7, after
150 which follicle cells undergo a programmed developmental switch to endocycles up until stage
151 10A (Margolis and Spradling 1995; Calvi *et al.* 1998). Given that there were two extra
152 endocycle genome doublings instead of the normal two mitotic divisions during the ~24 hours
153 from stage 4 / 5 to stage 6 / 7, these data also suggest that the duration of each induced
154 endocycle is approximately equal to that of the mitotic cycles that they supplanted (Margolis
155 and Spradling 1995). Moreover, the increased DNA content of these follicle cells at stage 10
156 suggests that starting endocycles early can override the undefined cell-autonomous
157 mechanisms that arrest endocycles to limit follicle cell ploidy to 16C.
158 We then examined the coordination of follicle cell cycles with later stages of oogenesis.
159 in wild type, different follicle cells arrest endocycles at different times of stage 9-10A when they
160 reach 16C. At the onset of stage 10B, follicle cells over the oocyte synchronously begin a
161 specialized DNA replication program of developmental gene amplification (Fig. 2A) (Spradling
162 and Mahowald 1980; Calvi *et al.* 1998). This selective gene amplification entails site-specific
163 rereplication of specific loci that encode eggshell and other proteins, a process that is required

164 for normal eggshell synthesis (Calvi and Spradling 1999; Calvi 2006; Hua and Orr-Weaver
165 2017). These rereplicating loci can be detected as distinct nuclear foci of EdU incorporation
166 beginning in stage 10B (Calvi *et al.* 1998). EdU labeling of *tj-GAL4 GAL80^{ts} /* + control ovaries
167 at 29°C showed that all follicle cells over the oocyte had the normal nuclear foci of EdU in
168 stage 10B, indicating that the onset of amplification had the normal synchrony among follicle
169 cells (Fig. 2F, H, H') (Calvi *et al.* 1998; Calvi and Lilly 2004). Follicle cells that had been
170 expressing Rux for 24 hours also had the normal transition to synchronous amplification in
171 stage 10B (Fig. 2G). At the time of temperature shift one day earlier, most of these follicle cells
172 would have already undergone the developmental switch to endocycles in stage 6 / 7, and
173 therefore do not represent premature endocycling cells (Fig 2A). In contrast, two days after a
174 temperature shift, the follicle cells in a stage 10B egg chamber are those that prematurely
175 switched to endocycles in stage 4 / 5 (Fig. 2A). These premature endocycles resulted in some
176 stage 10B egg chambers with a mixture of follicle cells that had either the normal amplification
177 foci or pan-nuclear EdU incorporation indicative of continued genomic replication (Fig. 2I-J).
178 The two-day delay in the onset of this phenotype suggests that starting endocycles early
179 disrupts the later arrest of endocycle genomic replication and transition to developmental gene
180 amplification.
181
182 <u>Premature endocycling inhibits border cell migration</u>
183 During stage 9, most follicle cells migrate posteriorly to a position over the oocyte.
184 Despite disruptions to cell structure and developmental amplification, this migration was
185 normal in egg chambers with prematurely endocycling follicle cells, with most follicle cells
186 achieving their normal position over the oocyte by stage 10A (Fig. 2C, C'). Unlike these main
187 body follicle cells, a small group of follicle cells delaminates from the anterior epithelium and
188 migrates posteriorly between the nurse cells (Montell *et al.* 1992; Spradling 1993; Montell *et al.*
189 2012; Mishra *et al.* 2019b). This collective migration event is initiated in early stage 9 when two
190 specialized follicle cells, known as the polar cells, recruit 4-6 neighboring follicle cells to
191 become border cells via JAK-STAT signaling (Montell *et al.* 1992; Silver and Montell 2001).
192 After arriving at their final destination at the anterior of the growing oocyte in stage 10A, this
193 migrating border cell cluster forms the sperm entry port known as the micropyle (King 1970;
194 Bishop and King 1984; Horne-Badovinac 2020). Because these border cells have been a

195 powerful model for collective cell migration during metastasis, we wished to investigate the
196 effect of premature endocycling on them (Stuelten *et al.* 2018).
197 We identified border cells based on their elevated E-cadherin levels and measured their
198 migration in both control and Rux-expressing stage 9-10A egg chambers two days after
199 induction at 29°C (Oda *et al.* 1997; Niewiadomska *et al.* 1999). We normalized border cell
200 migration to that of main body follicle cells on the surface of the same egg chamber during
201 stage 9-10A. In controls, the migration of the border cell cluster between the nurse cells stayed
202 on-pace with the anterior of the main body follicle cells, with both populations of follicle cells
203 reaching the oocyte by the onset of stage 10A (Fig. 3A, A′, C). In contrast, Rux expression
204 resulted in border cells lagging behind the main body follicle cells to varying extents (Fig. 3B-
205 C). In some egg chambers, border cells had failed to even delaminate from the epithelium at
206 the anterior pole of the egg chamber by stage 10 (Fig. 3C). Border cell migration was also
207 impaired when premature endocycles were induced by *cyclin A* RNAi or *fzr* over-expression
208 (Fig. S5A-C"). Moreover, using either *fru-GAL4* or *slbo-GAL4* drivers to induce high levels of
209 Rux expression specifically in border cells after the developmental transition of follicle cells to
210 endocycles in stage 6/7 did not impair border cell migration (Fig. S5D-I). These results indicate
211 that the border cell migration defect is not because of unknown, off-target activities of the Rux
212 protein, but rather a result of premature endocycling.
213 We used a *10XStat92E-DsRed* JAK-STAT transcriptional reporter to determine whether
214 the failure to delaminate and migrate was because of a disruption of JAK-STAT signaling from
215 polar cells to border cells (Silver *et al.* 2005; Bach *et al.* 2007). Both controls and *UAS-Rux*
216 expressing ovaries had DsRed expression in follicle cells at the anterior and posterior ends of
217 chambers, with the anterior signal narrowing to include only the border cell cluster by stages 9-
218 10 of oogenesis, consistent with previous reports (Bach *et al.* 2007; Mallart *et al.* 2022) (Figure
219 3D-E"). The border cells in Rux-expressing ovaries had higher DsRed expression, which is
220 likely due to higher copy number of the *10XStat92E-DsRed* reporter in these polyploid cells
221 (Fig. 3E-E″). These DsRed-positive border cell clusters had impaired migration, with some
222 failing to delaminate from the epithelium, suggesting that these defects are not because of a
223 failure in JAK-STAT signaling from polar cells to border cells.
224 To further investigate the border cell migration defect, we examined the morphology and
225 number of cells in the border cell clusters. Labeling for the polar cell marker protein Fasciclin III
226 (Fas III) showed that after two days of Rux expression most egg chambers had the normal two

227 polar cells, including those in which border cells migrated slowly or failed to delaminate from
228 the epithelium (Fig. 3F-G‴) (Ruohola *et al.* 1991). Co-labeling against E-cadherin suggested
229 that these migrating clusters had an overall normal structure and cell polarity (Fig. 3F-G‴).
230 Rux-expressing egg chambers often had border cell clusters with a reduced number of border
231 cells that failed to migrate normally (Fig. 3H). Given that it has been shown that a similar deficit
232 of cells can inhibit border cell cluster delamination and migration, this observation suggests
233 that the migration defect in these clusters is at least partially attributable to a reduced number
234 of border cells (Silver and Montell 2001; Ghiglione *et al.* 2008). However, some clusters with
235 the normal number of border cells also failed to migrate, suggesting that other properties of
236 premature endocycling cells also inhibit migration (Fig. 3H).
237
238 Premature endocycling impairs oocyte growth
239 We next examined whether premature follicle cell endocycles affected the growth of
240 late-stage egg chambers. As mentioned previously, the overall morphology of stage 10B egg
241 chambers from Rux-expressing females appeared similar to those from controls with main
242 body follicle cells undergoing the normal migration posteriorly to over the growing oocyte (Fig
243 4A-D). One day after temperature shift stage 10B egg chambers from Rux-expressing females
244 had oocytes of a similar size to controls (Fig. 4A, B, E). At the time of temperature shift one
245 day earlier, the follicle cells in these stage 10B egg chambers would have been in stage 6/7
246 and already switched to developmental endocycles. In contrast, two days after temperature
247 shift the oocytes in Rux-expressing stage 10B egg chambers was significantly smaller (Fig.
248 4C-E). The follicle cells in these stage 10B egg chambers represent those that had
249 prematurely switched to endocycles in stage 4 / 5, suggesting that unscheduled endocycles
250 impair oocyte growth. The egg chambers with smaller oocytes had a corresponding increase in
251 the size of the nurse cell compartment (Fig. 4F). The ploidy of these nurse cells was not
252 increased, suggesting that the enlarged nurse cell compartment was not because of enhanced
253 nurse cell growth through additional endocycles (Fig. 4G). Labeling with the lipophilic dye Nile
254 Red indicated that egg chambers with premature endocycling follicle cells had the normal
255 accumulation of lipid droplets in nurse cells during stage 10 and their normal rapid transfer into
256 the oocyte with the rest of the nurse cell contents during stages 11-12 (Fig. 4H-K). These
257 results suggest that the two extra follicle cell endocycles had non-autonomous effects on
258 oocyte growth before stage 11.

259 <u>Premature endocycling disrupts eggshell synthesis and causes embryo lethality and female</u>
260 <u>infertility</u>
261 We evaluated whether the observed effects of premature endocycles on oogenesis
262 would impact female fertility. It is known that defects in developmental gene amplification like
263 those observed in Rux-expressing ovaries result in thin eggshells and a defective underlying
264 vitelline membrane, ultimately causing dehydration and death of embryos (Calvi 2006). We
265 therefore examined whether premature endocycles impaired eggshell synthesis. Some of the
266 eggs laid by *UAS-Rux* females had thin and unhardened shells that resembled those from
267 females with known defects in gene amplification, a phenotype that increased in frequency
268 over one to three days (Fig. 5A, C, E; Fig. S6A, B) (Calvi 2006). Unlike wild type eggs, those
269 from *UAS-Rux* females with abnormal shells were permeable to the dye Neutral Red,
270 confirming a defect in eggshell and vitelline membrane synthesis (Figure 5B, D). Expression of
271 Rux in females also resulted in reduced egg hatching, a phenotype that increased in severity
272 over subsequent days of maternal Rux expression (Fig. 5F). This decrease in egg hatching
273 correlated with the increase in collapsed, dehydrated eggs, suggesting that defects in vitelline
274 membrane and eggshell synthesis were a significant cause of embryo lethality (Fig. 5E, F).
275 Prolonged expression of Rux also had a negative effect on egg production during oogenesis.
276 Finally, after three days of Rux expression there was a high frequency of ovarioles with
277 degenerating stage 8-9 egg chambers, a phenotype diagnostic of an ovarian stress response
278 known as the vitellogenic checkpoint (Fig. S6C, D) (Peterson *et al.* 2015; Serizier and McCall
279 2017). This timing suggests that in these ovaries a very early entry into endocycles during
280 stage 1 / 2 triggers a general stress response three days later in stage 8. All together, these
281 data indicate that premature follicle cell endocycles have deleterious effects on eggshell
282 synthesis, embryo viability, and female fertility.
283
284 **Discussion**
285 There is a growing appreciation that cells can switch from mitotic cycles to endocycles
286 in response to conditional signals, but the impact of this unscheduled switch on tissue growth
287 and function is only beginning to be understood. We have found that premature follicle cell
288 endocycles cause pleiotropic defects in oogenesis and severely compromise female fertility
289 (Fig. 6). Although follicle cells normally switch to endocycles at stage 6 / 7 of oogenesis,
290 inducing them to switch one day earlier in stage 4 / 5 resulted in aberrant cell and epithelial

291 morphology, impaired oocyte growth, and perturbed the cessation of endocycles and transition
292 to developmental gene amplification. These aberrant cell and tissue phenotypes are an inroad
293 to defining the mechanisms by which cell growth and cell cycles are normally coordinated with
294 stages of oogenesis. They also reveal the ways in which unscheduled endocycles can have
295 deleterious consequences for tissue function that may apply across organisms, including in
296 human disease.

297 Starting follicle cell endocycles early disrupted the later asynchronous, cell-autonomous
298 arrest of endocycles during stage 9 and the synchronous onset of amplification at stage 10B
299 (Calvi *et al.* 1998). Previous analyses of the endocycle to amplification transition has defined
300 conserved mechanisms that regulate cell cycles and DNA replication during development. This
301 transition is regulated by the E2F, RB, and Myb transcription factor families and the synchronous
302 onset of amplification in stage 10B requires activity of Cyclin E / CDK2 (Calvi *et al.* 1998;
303 Royzman *et al.* 1999; Bosco *et al.* 2001; Cayirlioglu *et al.* 2001; Beall *et al.* 2002; Beall *et al.*
304 2004; Calvi 2006). Further insight into the coordination of the endocycle to amplification
305 transition with stages of oogenesis came from the finding that it requires downregulation of Notch
306 signaling, which results in an obligate increase in the activity of the steroid hormone ecdysone
307 and downstream expression of the transcription factor *tramtrack*, whose expression before stage
308 10 is further repressed by the micro-RNA *mir7* (Sun *et al.* 2008; Huang *et al.* 2013; Jia *et al.*
309 2015). Despite these key findings, much remains unknown about the molecular mechanism of
310 endocycle arrest and the selective activation of amplification origins at precise times of
311 oogenesis. Our finding that prematurely endocycling follicle cells can exceed their normal 16C
312 DNA content by stage 10 suggests that their cell-autonomous endocycle arrest is not dependent
313 on a strict genomic DNA counting mechanism. Some of these follicle cells increased their DNA
314 content further through continued genomic replication past stage 10, which comprised the
315 amplification of chorion and other genes that are required for eggshell synthesis. This disruption
316 of amplification is likely the cause of the thin eggshells and embryo lethality that we observed,
317 which phenocopies mutants that are known to impair gene amplification (Calvi 2006). A
318 continued analysis of these induced endocycles may provide further insights into the molecular
319 mechanisms that coordinate the timely transitions of cell cycle and DNA replication programs
320 during development.

321 Although there was no evidence for a cell autonomous restriction on DNA content, there
322 was a conservation of total DNA among all follicle cells. In wild type, the main body follicle cells

323 in stage 10 collectively represented ~10,256 haploid genome equivalents (641 cells * 16 C),
324 whereas inducing premature endocycles resulted in egg chambers with fewer but more highly
325 polyploid cells that represented a comparable ~10,024 haploid genome equivalents (179 cells *
326 56 C). This DNA equivalency may simply be the result of swapping two mitotic cycles for two
327 premature endocycles of equal duration. However, a similar conservation of genome
328 equivalents has also been noted when damaged tissue is regenerated by unscheduled
329 endocycles, a process termed compensatory cellular hypertrophy (CGH) (Tamori and Deng
330 2013; Cohen *et al.* 2018). Thus, there may be constraints on tissue growth that are
331 proportional to genome equivalents, as previously suggested (Cohen *et al.* 2018).
332 Premature endocycles resulted in severely aberrant follicle cell morphology and an
333 irregular follicular epithelium. These phenotypes contrast with the uniform cell and epithelial
334 morphology of endocycling follicle cells from wild type ovaries. The basis for this difference
335 between induced and developmental endocycles is currently unclear. One possibility is that
336 induced and developmental endocycling cells differ in the pathways that coordinate their
337 morphology with their hypertrophic growth to large cell size. For example, it is known that the
338 activity of the Hippo-Yorkie growth pathway is coupled to multiple cell polarity and cell-cell
339 junction protein complexes (Zheng and Pan 2019). Although premature endocycles resulted in
340 aberrant cell shapes, sizes, and cell-cell contacts, we did not find clear evidence for a direct
341 effect of induced endocycles on cell polarity. However, this last question was difficult to
342 address given the highly aberrant cell morphology and a further investigation into the effects of
343 unscheduled endocycles on cell polarity may be warranted.
344 The aberrant follicular epithelium may be related to the global effects of premature
345 endocycles on egg chamber morphology. The deformations of the somatic follicle cell-germline
346 interface before stage 6 suggests that premature endocycles may uncouple the coordinated
347 growth of soma and underlying germline nurse cells, a process that is incompletely understood
348 (Vachias *et al.* 2014; Giedt and Tootle 2023). Premature follicle cell endocycles also had non-
349 autonomous effects on oocyte growth. Although stage 10 oocytes were smaller, the rapid
350 transfer of lipid droplets and other nurse cell contents during stage 11 was normal, as was final
351 egg size. These observations are consistent with a model wherein a somatic epithelium of
352 fewer and more highly polyploid follicle cells impedes the slow transport of nurse cell contents
353 into the growing oocyte before stage 11, but not the rapid transfer of nurse cell contents that
354 occurs during stage 11 (Giedt and Tootle 2023). Smaller stage 10 oocytes may also be the

355 result of a defect in vitellogenesis. This process entails paracellular transport of yolk protein
356 across the follicular epithelium via a process that is enabled by a regulated increase in
357 epithelial permeability beginning in stage 8, a state known as patency (Isasti-Sanchez *et al.*
358 2021; Riechmann 2021). Patency requires remodeling of cell-cell junctions through a
359 mechanism that includes E-cadherin, whose labeling was altered in premature endocycling
360 follicle cells (Horne-Badovinac and Bilder 2005; Isasti-Sanchez *et al.* 2021). Thus, the aberrant
361 cell and epithelial morphology of induced endocycling cells may disturb the remodeling of cell-
362 cell contacts that is required for patency and oocyte growth. More broadly, these results
363 suggest that unscheduled endocycles may affect the coordinated growth and regulated
364 permeability of epithelia in other tissues.

365 The highly penetrant negative effect of premature endocycles on border cell migration is
366 likely due, in part, to a reduced number of border cells in the clusters, which has previously
367 been shown to impair migration (Silver and Montell 2001; Silver *et al.* 2005; Ghiglione *et al.*
368 2008; Mishra *et al.* 2019a). Nonetheless, some clusters with the normal number of border cells
369 also failed to migrate, indicating that there are other mechanisms that inhibit delamination and
370 migration. Our observation of impaired collective border cell migration contrasts with evidence
371 that polyploidy enhances migration of cancer cells *in vitro* and may promote collective cell
372 migration during metastasis *in vivo* (Godinho *et al.* 2014; Wang *et al.* 2019; Mallin *et al.*
373 2023). An important implication of our observations, therefore, is that the effects of
374 unscheduled endocycles on cell migration may be dependent on cell type and tissue context. It
375 is also possible that oncogenic mutations in cancer cells may synergize with the polyploid state
376 to enhance migratory properties.

377 Overall, our study has revealed that unscheduled endocycles can have severe
378 pleiotropic effects on tissue growth and function. Further characterization of these effects will
379 lead to a greater understanding of how endocycling, both scheduled and unscheduled, can
380 promote tissue regeneration or contribute to disease.

Materials and Methods

<u>*Drosophila* genetics:</u> *w⁻; tj-GAL4 tub-GAL80^{ts} / CyO TwistGFP* flies were crossed to *w^{1118}* (control) or *w⁻; UAS-Rux / SM6a* (experimental) flies, and their offspring were reared at 18°C during larval and early adult development. The resulting adult female offspring were fed wet yeast with males for 2 days at 18°C before being transferred to new wet yeast and shifted to 29°C for 1, 2, or 3 days (as noted in the text). The females and males were transferred to new wet yeast every 2 days during the experiments. This process was replicated in the *UAS-CycA^{RNAi,} UAS-fzr*, and the *10XStatDsRed* experiments. Experiments with the *slbo-GAL4* and *fru-GAL4* border-cell-specific drivers were carried out at 25°C. The *w⁻; tj-GAL4 tub-GAL80^{ts} / CyO TwistGFP* strain was a generous gift from L. Weaver. The *w⁻; UAS-Rux / SM6a* strain was obtained from the Bloomington Drosophila Stock Center (BDSC #9166). The *w⁻; 10XStatDsRed* strain was a generous gift from E. Bach. The *w⁻; slbo-GAL4 10XUAS-CD8GFP* strain was obtained from the BDSC (BDSC #76363). The *w^{1118}; fru-GAL4* strain was obtained from the BDSC (BDSC #30027). The *w⁻; UAS-CycA^{RNAi}* strain was obtained from the Vienna *Drosophila* Resource Center (VDRC v32421). The *w⁻; hsp70-GAL4 UAS-fzr / CyO; UAS-fzr* (*2XUAS-fzr*) strain is available upon request, and its components are available from the BDSC (BDSC #91688 for *UAS-fzr* on chromosome II and BDSC #91689 for *UAS-fzr* on chromosome III). All fly strains are also enumerated in the Reagent Table.

<u>Immunofluorescence microscopy:</u> Ovaries were fixed and labeled as previously described (Schwed *et al.* 2002). For E-cadherin labeling, fixation buffers were supplemented with 1 mM $CaCl_2$. The following antibodies and dilutions were used: rat anti-Shg (fly E-cadherin), 1:20 (DSHB DCAD2); mouse anti-Arm (fly β-catenin), 1:100 (DSHB N2 7A1); rabbit anti-phosphorylated histone H3 (pH3), 1:1000 (Millipore 06-570); mouse anti-Dlg1, 1:200 (DSHB 4F3); mouse anti-FasIII, 1:50 (DSHB 7G10); rabbit anti-GFP, 1:1000 (Invitrogen A-11122). EdU incorporation *in vitro* was for 1 hour as previously described (Calvi and Lilly, 2004). For lipid droplet detection, 10mg/mL Nile Red stock was diluted 1:500 in blocking buffer, and ovaries were incubated for 1 hour at room temperature with nutating, as previously described (Giedt *et al.* 2023). Asynchronous chorion gene amplification was defined as stage 10B egg chambers with both punctate and pan-nuclear EdU labeling of follicle cell nuclei. Egg chambers with more than one pan-nuclear EdU labeled nucleus were scored as “asynchronous.” For the dye exclusion assay, eggs were incubated in 1mL of 5 mg/mL of Neutral Red for 10 minutes, as

412 previously described (LeMosy and Hashimoto 2000). Fluorescence micrographs were taken on
413 a Leica SP8 confocal or a Leica DM5500 B. DIC images of stage 10B egg chambers were
414 taken using a Leica DM5500 B. Brightfield images of laid eggs were taken using a Zeiss
415 SteREO Discovery.V12. Nuclear DNA content was quantified using ImageJ/FIJI by measuring
416 mean DAPI fluorescence per pixel in a nucleus, subtracting local mean background DAPI
417 fluorescence per pixel, and then multiplying the difference by the number of pixels per nucleus
418 to obtain the corrected total DAPI fluorescence intensity. To quantify the number of follicle cells
419 per egg chamber, z-stacks of entire egg chambers were imaged, then DAPI-labeled nuclei
420 were manually counted for the top part of the egg chamber where nuclei were most
421 distinguishable from each other. This follicle cell count was then doubled to estimate the total
422 number of follicle cells per egg chamber. The number of pH-positive follicle cells in early-stage
423 egg chambers, total number of follicle cells in late-stage egg chambers, oocyte area, nurse cell
424 compartment length, follicle cell diameter (along their longest axis), and border cell migration
425 were quantified using ImageJ/FIJI.

426 Eggshell scoring and egg hatch rate: Eggs from well-fed and mated females were collected on
427 grape plates with a thin layer of yeast paste for 2-4 hours for each respective day of 29°C
428 transgene induction. Eggs were scored as having “thin” chorions if they met the following
429 criteria: 1) The eggshell appeared mucosal with no obvious follicle cell footprint pattern, 2) they
430 had flaccid dorsal appendages, and / or 3) they were dehydrated and burst easily after a light
431 touch with a paintbrush. The validity of these criteria and permeability of eggshell and vitelline
432 membrane were independently confirmed by the Neutral Red staining described above. For
433 hatch rates, eggs were lined up and incubated at 18°C to ensure no GAL4-driven transgene
434 expression affected their viability. They were then scored for hatching over four subsequent
435 days.

436 Statistical Analysis: Data graphing and statistical analyses were carried out in GraphPad
437 Prism. Data were tested for normality and homoscedasticity to determine correct analyses.
438 Sample size (n) is defined as the total of independent observations / measurements used for
439 the chosen analysis across multiple biological replicates. All averages shown are mean ± s.d.,
440 except for Figure 2J, which is mean ± s.e.m, and Figure 4G, which is median. Two-tailed
441 Mann-Whitney tests were used to test for significance in Figs. 1F, S1E-F, 2D, 4E, and 4G.
442 Figure 4E was corrected for multiple comparisons. A two-tailed Welch’s t-test was used to test

443 for significance in Figs. 1G & 2E. A two-tailed unpaired t-test was used to test for significance
444 in Fig. 2J. A Mixed Effects Two-Way ANOVA was used to test for significance in Fig. 4F.

445 **Data availability**

446 Fly strains used are enumerated in the article. All fly strains used in the study are publicly
447 available at the Bloomington Drosophila Stock Center, or upon request. All reagents used in
448 this study are publicly available.

449 **Acknowledgements**

450 We thank S. Brown and Y.T. Huang for experimental assistance. We are appreciative of the
451 thoughtful feedback from S. Brown, L. Hesting, Y.T. Huang, P. Rangarajan, and C. Walczak, as
452 well as from the editor and anonymous reviewers. We thank A. Kun and J. Powers of the IU
453 Light Microscopy Imaging Center. Special thanks to D. Montell for advice and E. Bach and L.
454 Weaver for fly strains

455 **Competing Interests**

456 The authors declare no competing interests.

457 **Author Contributions**

458 H.C.H. performed experiments and statistical analyses. Both authors wrote and edited the
459 manuscript. B.R.C. secured funding and provided mentorship and supervision.

460 **Funding**

461 This work was supported by National Institutes of Health Grant NIH R01GM113107 to B.R.C.

462 **References**

463 Almeida Machado Costa, C., X. F. Wang, C. Ellsworth and W. M. Deng, 2022 Polyploidy in
464 development and tumor models in Drosophila. Semin Cancer Biol 81**:** 106-118.
465 Avedisov, S. N., I. Krasnoselskaya, M. Mortin and B. J. Thomas, 2000 Roughex mediates G(1)
466 arrest through a physical association with cyclin A. Mol Cell Biol 20**:** 8220-8229.
467 Bach, E. A., L. A. Ekas, A. Ayala-Camargo, M. S. Flaherty, H. Lee *et al.*, 2007 GFP reporters
468 detect the activation of the Drosophila JAK/STAT pathway in vivo. Gene Expr Patterns
469 7**:** 323-331.
470 Bailey, E. C., S. Kobielski, J. Park and V. P. Losick, 2021 Polyploidy in Tissue Repair and
471 Regeneration. Cold Spring Harb Perspect Biol 13.
472 Beall, E. L., M. Bell, D. Georlette and M. R. Botchan, 2004 Dm-myb mutant lethality in
473 Drosophila is dependent upon mip130: positive and negative regulation of DNA
474 replication. Genes Dev 18**:** 1667-1680.
475 Beall, E. L., J. R. Manak, S. Zhou, M. Bell, J. S. Lipsick *et al.*, 2002 Role for a Drosophila Myb-
476 containing protein complex in site-specific DNA replication. Nature 420**:** 833-837.
477 Besen-McNally, R., K. J. Gjelsvik and V. P. Losick, 2021 Wound-induced polyploidization is
478 dependent on Integrin-Yki signaling. Biol Open 10.
479 Bishop, D. L., and R. C. King, 1984 An ultrastructural study of ovarian development in the otu-7
480 mutant of Drosophila melanogaster. J. Cell Sci. 67**:** 87-119.
481 Bosco, G., W. Du and T. L. Orr-Weaver, 2001 DNA replication control through interaction of
482 E2F-RB and the origin recognition complex. Nat Cell Biol 3**:** 289-295.
483 Brand, A., and N. Perrimon, 1993 Targeted gene expression as a means of altering cell fates
484 and generating dominant phenotypes. Development 118**:** 401-415.
485 Brennan, M. D., A. J. Weiner, T. J. Goralski and A. P. Mahowald, 1982 The follicle cells are a
486 major site of vitellogenin synthesis in Drosophila melanogaster. Dev Biol 89**:** 225-236.
487 Cadart, C., and R. Heald, 2022 Scaling of biosynthesis and metabolism with cell size.
488 Molecular Biology of the Cell 33**:** pe5.
489 Calvi, B. R., 2006 Developmental DNA amplification, pp. 233-255. in *DNA replication and*
490 *human disease*, edited by M. L. DePamphilis. Cold Spring Harbor Laboratory Press,
491 Cold Spring Harbor, NY.
492 Calvi, B. R., 2013 Making big cells: one size does not fit all. Proc Natl Acad Sci U S A 110**:**
493 9621-9622.
494 Calvi, B. R., and M. A. Lilly, 2004 BrdU labeling and nuclear flow sorting of the Drosophila
495 ovary, pp. 203-213 in *Drosophila Cytogenetics Protocols*, edited by D. Henderson.
496 Humana Press, Totowa.
497 Calvi, B. R., M. A. Lilly and A. C. Spradling, 1998 Cell cycle control of chorion gene
498 amplification. Genes Dev 12**:** 734-744.
499 Calvi, B. R., and A. C. Spradling, 1999 Chorion gene amplification in Drosophila: A model for
500 metazoan origins of DNA replication and S-phase control. Methods 18**:** 407-417.
501 Cayirlioglu, P., P. C. Bonnette, M. R. Dickson and R. J. Duronio, 2001 Drosophila E2f2
502 promotes the conversion from genomic DNA replication to gene amplification in ovarian
503 follicle cells. Development 128**:** 5085-5098.
504 Cohen, E., S. R. Allen, J. K. Sawyer and D. T. Fox, 2018 Fizzy-Related dictates A cell cycle
505 switch during organ repair and tissue growth responses in the Drosophila hindgut. Elife
506 7.

507 Deng, W. M., C. Althauser and H. Ruohola-Baker, 2001 Notch-Delta signaling induces a
508 transition from mitotic cell cycle to endocycle in Drosophila follicle cells. Development
509 128: 4737-4746.
510 Duhart, J. C., T. T. Parsons and L. A. Raftery, 2017 The repertoire of epithelial morphogenesis
511 on display: Progressive elaboration of Drosophila egg structure. Mech Dev 148: 18-39.
512 Fadiga, J., and T. G. Nystul, 2019 The follicle epithelium in the Drosophila ovary is maintained
513 by a small number of stem cells. Elife 8.
514 Fox, D. T., D. E. Soltis, P. S. Soltis, T. L. Ashman and Y. Van de Peer, 2020 Polyploidy: A
515 Biological Force From Cells to Ecosystems. Trends Cell Biol 30: 688-694.
516 Gandara, A. C. P., and D. Drummond-Barbosa, 2022 Warm and cold temperatures have
517 distinct germline stem cell lineage effects during Drosophila oogenesis. Development
518 149.
519 Ghiglione, C., O. Devergne, D. Cerezo and S. Noselli, 2008 Drosophila RalA is essential for
520 the maintenance of Jak/Stat signalling in ovarian follicles. EMBO Rep 9: 676-682.
521 Giedt, M. S., J. M. Thomalla, R. P. White, M. R. Johnson, Z. W. Lai *et al.*, 2023 Adipose
522 triglyceride lipase promotes prostaglandin-dependent actin remodeling by regulating
523 substrate release from lipid droplets. Development 150.
524 Giedt, M. S., and T. L. Tootle, 2023 The Vast Utility of Drosophila Oogenesis. Methods Mol Biol
525 2626: 1-36.
526 Godinho, S. A., R. Picone, M. Burute, R. Dagher, Y. Su *et al.*, 2014 Oncogene-like induction of
527 cellular invasion from centrosome amplification. Nature 510: 167-171.
528 Godt, D., and U. Tepass, 1998 Drosophila oocyte localization is mediated by differential
529 cadherin-based adhesion. Nature 395: 387-391.
530 Gonzalez-Reyes, A., and D. St Johnston, 1998 The Drosophila AP axis is polarised by the
531 cadherin-mediated positioning of the oocyte. Development 125: 3635-3644.
532 Hassel, C., B. Zhang, M. Dixon and B. R. Calvi, 2014 Induction of endocycles represses
533 apoptosis independently of differentiation and predisposes cells to genome instability.
534 Development 141: 112-123.
535 Herriage, H. C., Y. T. Huang and B. R. Calvi, 2023 The antagonistic relationship between
536 apoptosis and polyploidy in development and cancer. Semin Cell Dev Biol.
537 Horne-Badovinac, S., 2020 The Drosophila micropyle as a system to study how epithelia build
538 complex extracellular structures. Philos Trans R Soc Lond B Biol Sci 375: 20190561.
539 Hua, B. L., and T. L. Orr-Weaver, 2017 DNA Replication Control During Drosophila
540 Development: Insights into the Onset of S Phase, Replication Initiation, and Fork
541 Progression. Genetics 207: 29-47.
542 Huang, Y. C., L. Smith, J. Poulton and W. M. Deng, 2013 The microRNA miR-7 regulates
543 Tramtrack69 in a developmental switch in Drosophila follicle cells. Development 140:
544 897-905.
545 Jia, D., Y. C. Huang and W. M. Deng, 2015 Analysis of Cell Cycle Switches in Drosophila
546 Oogenesis. Methods Mol Biol 1328: 207-216.
547 Khoury, M. J., and D. Bilder, 2020 Distinct activities of Scrib module proteins organize epithelial
548 polarity. Proc Natl Acad Sci U S A 117: 11531-11540.
549 King, R. C., 1970 *Ovarian Development in Drosophila melanogaster*. Academic Press, New
550 York.
551 LeMosy, E. K., and C. Hashimoto, 2000 The nudel protease of Drosophila is required for
552 eggshell biogenesis in addition to embryonic patterning. Dev Biol 217: 352-361.

553 Lopez-Schier, H., and D. St Johnston, 2001 Delta signaling from the germ line controls the
554 proliferation and differentiation of the somatic follicle cells during Drosophila oogenesis.
555 Genes Dev 15**:** 1393-1405.
556 Mallart, C., F. Chalvet, S. Netter, A. Y. Torres, M. Poidevin *et al.*, 2022 E-cadherin acts as a
557 positive regulator of the JAK-STAT signaling pathway during Drosophila oogenesis.
558 Front Cell Dev Biol 10**:** 886312.
559 Mallin, M. M., N. Kim, M. I. Choudhury, S. J. Lee, S. S. An *et al.*, 2023 Cells in the
560 polyaneuploid cancer cell (PACC) state have increased metastatic potential. Clin Exp
561 Metastasis 40**:** 321-338.
562 Margolis, J., and A. Spradling, 1995 Identification and behavior of epithelial stem cells in the
563 Drosophila ovary. Development 121**:** 3797-3807.
564 McGuire, S. E., Z. Mao and R. L. Davis, 2004 Spatiotemporal gene expression targeting with
565 the TARGET and gene-switch systems in Drosophila. Sci STKE 2004**:** pl6.
566 Merkle, J. A., J. Wittes and T. Schupbach, 2020 Signaling between somatic follicle cells and
567 the germline patterns the egg and embryo of Drosophila. Curr Top Dev Biol 140**:** 55-86.
568 Mishra, A. K., J. P. Campanale, J. A. Mondo and D. J. Montell, 2019a Cell interactions in
569 collective cell migration. Development 146.
570 Mishra, A. K., J. A. Mondo, J. P. Campanale and D. J. Montell, 2019b Coordination of
571 protrusion dynamics within and between collectively migrating border cells by myosin II.
572 Mol Biol Cell 30**:** 2490-2502.
573 Montell, D. J., P. Rorth and A. C. Spradling, 1992 slow border cells, a locus required for a
574 developmentally regulated cell migration during oogenesis, encodes Drosophila C/EBP.
575 Cell 71**:** 51-62.
576 Montell, D. J., W. H. Yoon and M. Starz-Gaiano, 2012 Group choreography: mechanisms
577 orchestrating the collective movement of border cells. Nat Rev Mol Cell Biol 13**:** 631-
578 645.
579 Niewiadomska, P., D. Godt and U. Tepass, 1999 DE-Cadherin is required for intercellular
580 motility during Drosophila oogenesis. J Cell Biol 144**:** 533-547.
581 Oda, H., T. Uemura and M. Takeichi, 1997 Phenotypic analysis of null mutants for DE-cadherin
582 and Armadillo in Drosophila ovaries reveals distinct aspects of their functions in cell
583 adhesion and cytoskeletal organization. Genes Cells 2**:** 29-40.
584 Ovrebo, J. I., and B. A. Edgar, 2018 Polyploidy in tissue homeostasis and regeneration.
585 Development 145.
586 Peterson, J. S., A. K. Timmons, A. A. Mondragon and K. McCall, 2015 The End of the
587 Beginning: Cell Death in the Germline. Curr Top Dev Biol 114**:** 93-119.
588 Pienta, K. J., E. U. Hammarlund, R. H. Austin, R. Axelrod, J. S. Brown *et al.*, 2022 Cancer cells
589 employ an evolutionarily conserved polyploidization program to resist therapy. Semin
590 Cancer Biol 81**:** 145-159.
591 Raikhel, A. S., and T. S. Dhadialla, 1992 Accumulation of yolk proteins in insect oocytes. Annu
592 Rev Entomol 37**:** 217-251.
593 Rotelli, M. D., R. A. Policastro, A. M. Bolling, A. W. Killion, A. J. Weinberg *et al.*, 2019 A Cyclin
594 A-Myb-MuvB-Aurora B network regulates the choice between mitotic cycles and
595 polyploid endoreplication cycles. PLoS Genet 15**:** e1008253.
596 Royzman, I., R. J. Austin, G. Bosco, S. P. Bell and T. L. Orr-Weaver, 1999 ORC localization in
597 Drosophila follicle cells and the effects of mutations in *dE2F* and *dDP*. Genes Dev 13**:**
598 827-840.

599 Ruohola, H., K. Bremer, D. Baker, J. Swedlow, L. Jan *et al.*, 1991 Role of neurogenic genes in
600 establishment of follicle cell fate and oocyte polarity during oogenesis in Drosophila.
601 Cell 66**:** 433-449.
602 Schwed, G., N. May, Y. Pechersky and B. R. Calvi, 2002 Drosophila minichromosome
603 maintenance 6 is required for chorion gene amplification and genomic replication. Mol
604 Biol Cell 13**:** 607-620.
605 Serizier, S. B., and K. McCall, 2017 Scrambled Eggs: Apoptotic Cell Clearance by Non-
606 Professional Phagocytes in the Drosophila Ovary. Front Immunol 8**:** 1642.
607 Shu, Z., S. Row and W. M. Deng, 2018 Endoreplication: The Good, the Bad, and the Ugly.
608 Trends Cell Biol 28**:** 465-474.
609 Silver, D. L., E. R. Geisbrecht and D. J. Montell, 2005 Requirement for JAK/STAT signaling
610 throughout border cell migration in Drosophila. Development 132**:** 3483-3492.
611 Silver, D. L., and D. J. Montell, 2001 Paracrine signaling through the JAK/STAT pathway
612 activates invasive behavior of ovarian epithelial cells in Drosophila. Cell 107**:** 831-841.
613 Spradling, A., and A. Mahowald, 1980 Amplification of genes for chorion proteins during
614 oogenesis in Drosophila melanogaster. Proc Natl Acad Sci U S A 77**:** 1096-1100.
615 Spradling, A. C., 1993 Developmental Genetics of Oogenesis in *The Development of*
616 *Drosophila melanogaster*, edited by M. B. a. A. Martinez-Arias. Cold Spring Harbor
617 Press, Cold Spring Harbor, New York.
618 Sprenger, F., N. Yakubovich and P. H. O'Farrell, 1997 S-phase function of Drosophila cyclin A
619 and its downregulation in G1 phase. Curr Biol 7**:** 488-499.
620 Stormo, B. M., and D. T. Fox, 2019 Interphase cohesin regulation ensures mitotic fidelity after
621 genome reduplication. Mol Biol Cell 30**:** 219-227.
622 Stuelten, C. H., C. A. Parent and D. J. Montell, 2018 Cell motility in cancer invasion and
623 metastasis: insights from simple model organisms. Nat Rev Cancer 18**:** 296-312.
624 Sun, J., and W. M. Deng, 2005 Notch-dependent downregulation of the homeodomain gene
625 cut is required for the mitotic cycle/endocycle switch and cell differentiation in
626 Drosophila follicle cells. Development 132**:** 4299-4308.
627 Sun, J., and W. M. Deng, 2007 Hindsight mediates the role of notch in suppressing hedgehog
628 signaling and cell proliferation. Dev Cell 12**:** 431-442.
629 Sun, J., L. Smith, A. Armento and W. M. Deng, 2008 Regulation of the endocycle/gene
630 amplification switch by Notch and ecdysone signaling. J Cell Biol 182**:** 885-896.
631 Tamori, Y., and W. M. Deng, 2013 Tissue repair through cell competition and compensatory
632 cellular hypertrophy in postmitotic epithelia. Dev Cell 25**:** 350-363.
633 Tepass, U., E. Gruszynski-DeFeo, T. A. Haag, L. Omatyar, T. Torok *et al.*, 1996 shotgun
634 encodes Drosophila E-cadherin and is preferentially required during cell rearrangement
635 in the neurectoderm and other morphogenetically active epithelia. Genes Dev 10**:** 672-
636 685.
637 Thomas, B. J., D. A. Gunning, J. Cho and L. Zipursky, 1994 Cell cycle progression in the
638 developing Drosophila eye: roughex encodes a novel protein required for the
639 establishment of G1. Cell 77**:** 1003-1014.
640 Uemura, T., H. Oda, R. Kraut, S. Hayashi, Y. Kotaoka *et al.*, 1996 Zygotic Drosophila E-
641 cadherin expression is required for processes of dynamic epithelial cell rearrangement
642 in the Drosophila embryo. Genes Dev 10**:** 659-671.
643 Vachias, C., C. Fritsch, P. Pouchin, O. Bardot and V. Mirouse, 2014 Tight coordination of
644 growth and differentiation between germline and soma provides robustness for
645 drosophila egg development. Cell Rep 9**:** 531-541.

646 Vidwans, S. J., P. J. DiGregorio, A. W. Shermoen, B. Foat, J. Iwasa *et al.*, 2002 Sister
647 chromatids fail to separate during an induced endoreplication cycle in Drosophila
648 embryos. Curr Biol 12**:** 829-833.
649 Wang, X., M. Zheng, F. Fei, C. Li, J. Du *et al.*, 2019 EMT-related protein expression in
650 polyploid giant cancer cells and their daughter cells with different passages after
651 triptolide treatment. Med Oncol 36**:** 82.
652 Weaver, L. N., T. Ma and D. Drummond-Barbosa, 2020 Analysis of Gal4 Expression Patterns
653 in Adult Drosophila Females. G3 (Bethesda) 10**:** 4147-4158.
654 Woods, D. F., C. Hough, D. Peel, G. Callaini and P. J. Bryant, 1996 Dlg protein is required for
655 junction structure, cell polarity, and proliferation control in Drosophila epithelia. J Cell
656 Biol 134**:** 1469-1482.
657 Zheng, Y., and D. Pan, 2019 The Hippo Signaling Pathway in Development and Disease. Dev
658 Cell 50**:** 264-282.

659

660 **Figure Legends**

661 **Figure 1: Premature endocycling disrupts early-stage follicular epithelial structure.** (A)
662 Drawing of an ovariole with select stages of oogenesis and follicle cell cycle transitions
663 indicated below. Follicle cells are pink. (B-C″) DAPI staining and immunolabeling against E-
664 cadherin in control (B-B″) or Rux-expressing (C-C″) early-stage egg chambers after two days
665 of incubation at 29°C. Stages (S) of oogenesis and germarium (G) are indicated. Scale bar =
666 15 μm. (D-E″) DAPI staining and immunolabeling against E-cadherin in cross-section images
667 through the follicle cell epithelium on the surface of control (D-D″) or Rux-expressing (E-E″)
668 stage 4 / 5 egg chambers after two days of incubation at 29°C. (F) Quantification of DNA
669 Content (C) from control and Rux-expressing stage 4 / 5 egg chambers after two days of
670 incubation at 29°C; ****$p < 0.0001$; n = 25 nuclei for control and n = 15 nuclei for *UAS-Rux*
671 across three biological replicates. (G) Quantification of cell diameter from control and Rux-
672 expressing stage 4 / 5 egg chambers after two days of incubation at 29°C. ****$p < 0.0001$; n =
673 49 cells for control and n = 28 cells for *UAS-Rux* across three biological replicates.

674 **Figure 2: Premature endocycling increases follicle cell polyploidy and disrupts the**
675 **endocycle-amplification transition.** (A) An experimental timeline of the temperature shift
676 experiments in relationship to the timing of egg chamber maturation. Select stages of
677 oogenesis, follicle cell cycle transitions, and their approximate duration during oogenesis are
678 indicated below. Follicle cells are pink. (B-C′) DAPI staining and immunolabeling against E-
679 cadherin in control (B, B′) and Rux-expressing stage 10B egg chambers (C, C′); scale bar = 30
680 μm. (D) Quantification of DNA Content in control and Rux-expressing stage 10B egg
681 chambers.; ****$p < 0.0001$; n = 85 nuclei in control and n = 104 nuclei in *UAS-Rux* across four
682 biological replicates. (E) Quantification of number of follicle cells in control and Rux-expressing
683 stage 10B egg chambers; ****$p < 0.0001$; n = 12 egg chambers in both across four biological
684 replicates. (F-I′) DAPI staining and EdU labeling of DNA replication in control (F, H, H′) and
685 Rux-expressing (G, I, I′) stage 10B egg chambers after one (F, G) or two (H-I′) days of
686 incubation at 29°C; scale bar = 25 μm (F, G, H, I) or 10 μm (H′, I′). (J) Quantification of percent
687 stage 10B egg chambers that had follicle cells with pan-nuclear EdU labeling in control and
688 Rux-expressing ovaries after 2 days of Rux expression. ***$p = 0.0003$; n = 26 egg chambers
689 for control and n = 19 egg chambers for *UAS-Rux* across three biological replicates.

690 **Figure 3: Premature endocycling inhibits border cell migration.** (A-B′) DAPI staining and
691 immunolabeling against E-cadherin in control (A, A′) and Rux-expressing (B, B′) egg chambers
692 after two days of incubation at 29°C; scale bar = 30 µm (A, B) or 15 µm (A′, B′). White arrows
693 indicate border cell clusters. White lines indicate extent of migration of border cell clusters, and
694 red lines indicate extent of migration of main body cells. (C) Quantification of border cell
695 migration at different times of stage 9 from control and Rux-expressing females after two days
696 of incubation at 29°C across five biological replicates. Each dot represents one egg chamber
697 with the distance migrated by its main body and border cells plotted on the x- and y-axis,
698 respectively. (D-E″) Expression of a JAK-STAT transcriptional reporter,*10XStatDsRed*, in
699 control ovaries (D-D″) and ovaries expressing *UAS-Rux* (E-E″) after two days of incubation at
700 29°C. White arrows indicate anterior follicle cells and migrating border cell clusters in controls
701 while red arrows indicate anterior follicle cells and delayed border cell clusters in Rux-
702 expressing egg chambers. Scale bar = 50 µm. (F-G‴) High magnification images of control (F-
703 F‴) or Rux-expressing (G-G‴) border cell clusters after two days of incubation at 29°C.
704 Clusters are visualized with DAPI staining and immunolabeling against FasIII and E-cadherin;
705 scale bar = 10 µm. (H) Quantification of border cell number vs. border cell percent migration
706 relative to main body cells in control and Rux-expressing ovaries. Each dot represents one egg
707 chamber.

708 **Figure 4: Premature endocycling of the follicular epithelium compromises germline**
709 **growth.** (A-D) Differential interference contrast images of control (A, C) and Rux-expressing
710 (B, D) stage 10B egg chambers after one (A, B) or two (C, D) days of incubation at 29°C. The
711 arrows indicate the posterior of egg chambers with the growing oocyte. scale bar = 100 µm.
712 (E) Quantification of oocyte area in control and Rux-expressing stage 10 egg chambers.; *$p <$
713 0.05; for day one, n = 13 oocytes for control and n = 15 oocytes for *UAS-Rux* across three
714 biological replicates; for day 2, n = 20 oocytes for control and n = 24 oocytes for *UAS-Rux*
715 across five biological replicates. (F) Quantification of nurse cell compartment length; **$p =$
716 0.0021, ***$p = 0.0002$, ****$p < 0.0001$. For day 1, n = 20 egg chambers for control and UAS-
717 *Rux* across three biological replicates; for day 2, n = 27 egg chambers for control and n = 30
718 egg chambers for *UAS-Rux* across five biological replicates. (G) Quantification of Stage 10
719 nurse cell ploidy. For control, n = 53 nurse cell nuclei; for Rux, n = 59 nurse cell nuclei. (H-K)

720 DAPI staining of nuclei and Nile Red staining of lipid droplets in Stage 10B (H, I) or Stage 13
721 (J, K) egg chambers. Scale bar = 50 μm (H, I) or 100 μm (J, K).

722 **Figure 5: Premature endocycling disrupts eggshell synthesis and causes embryo**
723 **lethality.** (A-D) Brightfield images of eggs laid by control (A, B) and Rux-expressing females
724 (C, D) after two days of incubation at 29°C; scale bar = 200 μm. Neutral red labeling is shown
725 in grayscale (B, D). Quantification of percent of eggs with thin shells (E) and hatch rate (F)
726 across three biological replicates.

727 **Figure 6: Premature endocycling causes pleiotropic defects in oogenesis.** Premature
728 entry of follicle cells (pink) into the endocycle causes aberrant cell and epithelial structure in
729 early stages of oogenesis. These egg chambers with premature endocycles develop into later
730 stages of oogenesis and have multiple defects including failure of border cell migration,
731 disrupted endocycle to amplification transition, and non-autonomous effects on germline
732 growth. The delay in these later defects after temperature shift indicate that they are the result
733 a premature switch to endocycles in earlier.

FIGURE 1

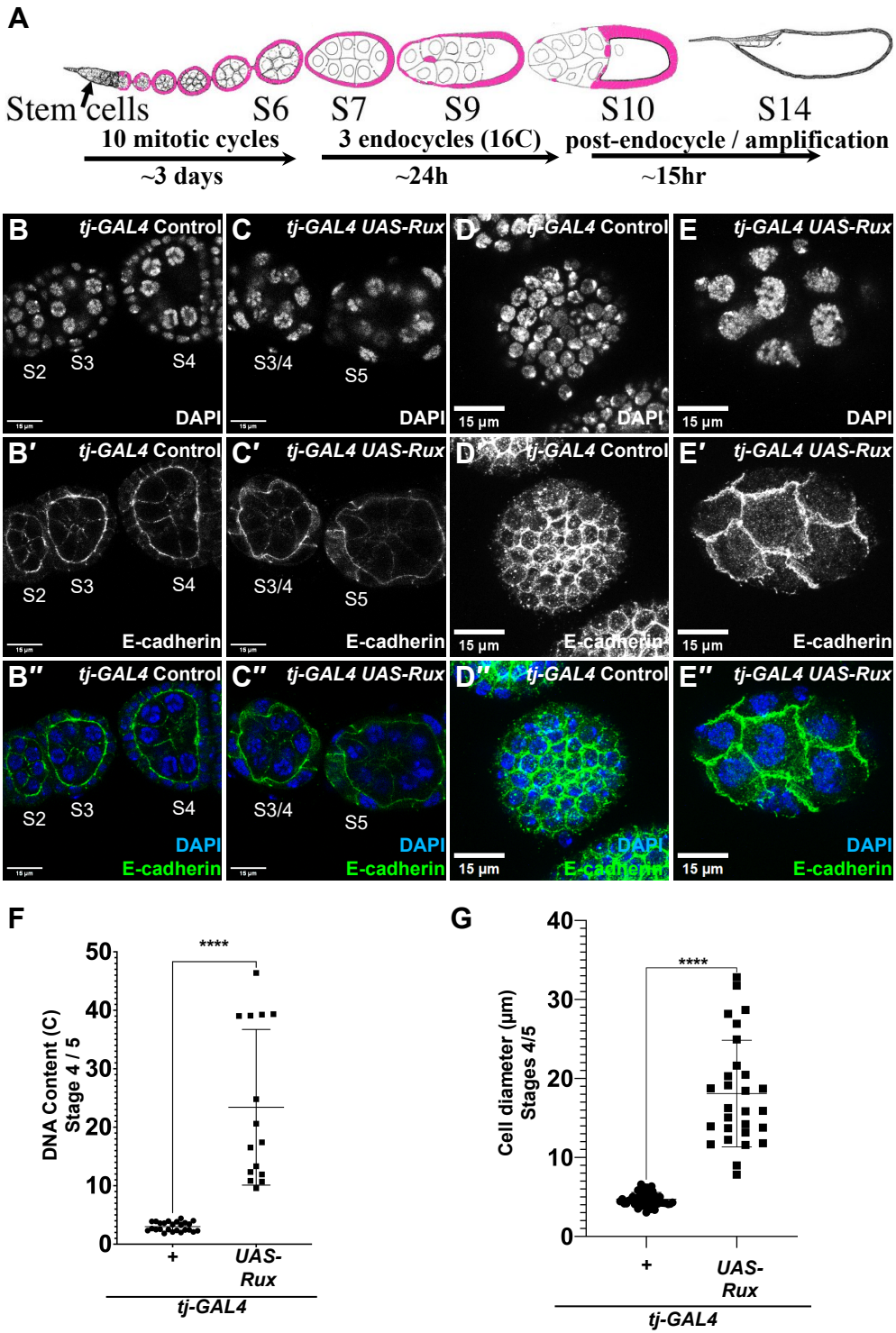
A
Stem cells
S6
S7
S9
S10
S14
10 mitotic cycles
~3 days
3 endocycles (16C)
~24h
post-endocycle / amplification
~15hr
B tj-GAL4 Control
C tj-GAL4 UAS-Rux
D tj-GAL4 Control
E tj-GAL4 UAS-Rux
S2
S3
S4
S3/4
S5
DAPI
15 µm
B′ tj-GAL4 Control
C′ tj-GAL4 UAS-Rux
D′ tj-GAL4 Control
E′ tj-GAL4 UAS-Rux
E-cadherin
B″ tj-GAL4 Control
C″ tj-GAL4 UAS-Rux
D″ tj-GAL4 Control
E″ tj-GAL4 UAS-Rux
DAPI
E-cadherin
F
DNA Content (C)
Stage 4 / 5
****
+
UAS-Rux
tj-GAL4
G
Cell diameter (µm)
Stages 4/5
****
+
UAS-Rux
tj-GAL4

Figure 2

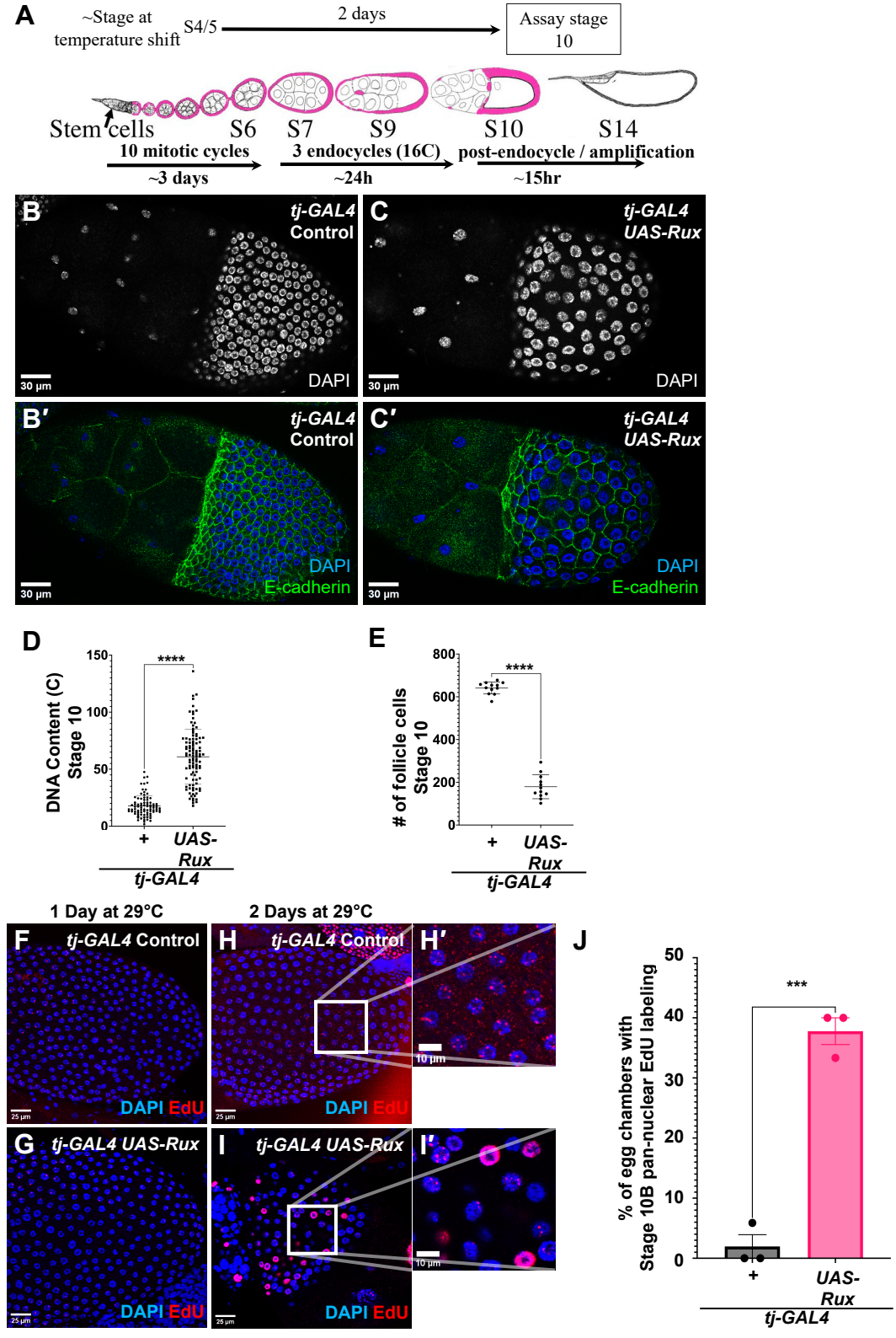
A
~Stage at temperature shift
S4/5
2 days
Assay stage 10
Stem cells
S6
S7
S9
S10
S14
10 mitotic cycles
~3 days
3 endocycles (16C)
~24h
post-endocycle / amplification
~15hr
B
tj-GAL4 Control
DAPI
30 µm
C
tj-GAL4 UAS-Rux
DAPI
30 µm
B′
tj-GAL4 Control
DAPI
E-cadherin
30 µm
C′
tj-GAL4 UAS-Rux
DAPI
E-cadherin
30 µm
D
DNA Content (C) Stage 10
150
100
50
0
****
+
UAS-Rux
tj-GAL4
E
# of follicle cells Stage 10
800
600
400
200
0
****
+
UAS-Rux
tj-GAL4
1 Day at 29°C
2 Days at 29°C
F
tj-GAL4 Control
DAPI EdU
25 µm
H
tj-GAL4 Control
DAPI EdU
25 µm
H′
10 µm
G
tj-GAL4 UAS-Rux
DAPI EdU
25 µm
I
tj-GAL4 UAS-Rux
DAPI EdU
25 µm
I′
10 µm
J
% of egg chambers with Stage 10B pan-nuclear EdU labeling
50
40
30
20
10
0
***
+
UAS-Rux
tj-GAL4

FIGURE 3

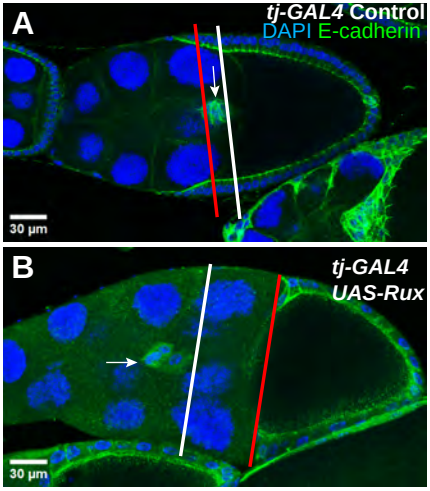
A
tj-GAL4 Control
DAPI E-cadherin
30 µm
B
tj-GAL4
UAS-Rux
30 µm

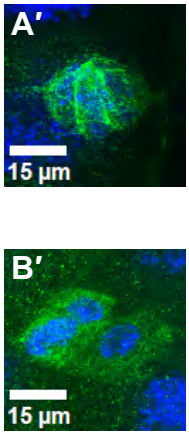
A′
15 µm
B′
15 µm

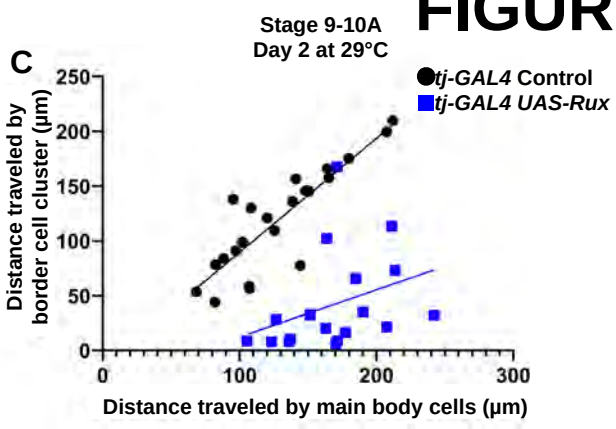
C
Stage 9-10A
Day 2 at 29°C
tj-GAL4 Control
tj-GAL4 UAS-Rux
Distance traveled by border cell cluster (µm)
Distance traveled by main body cells (µm)
0
50
100
150
200
250
0
100
200
300

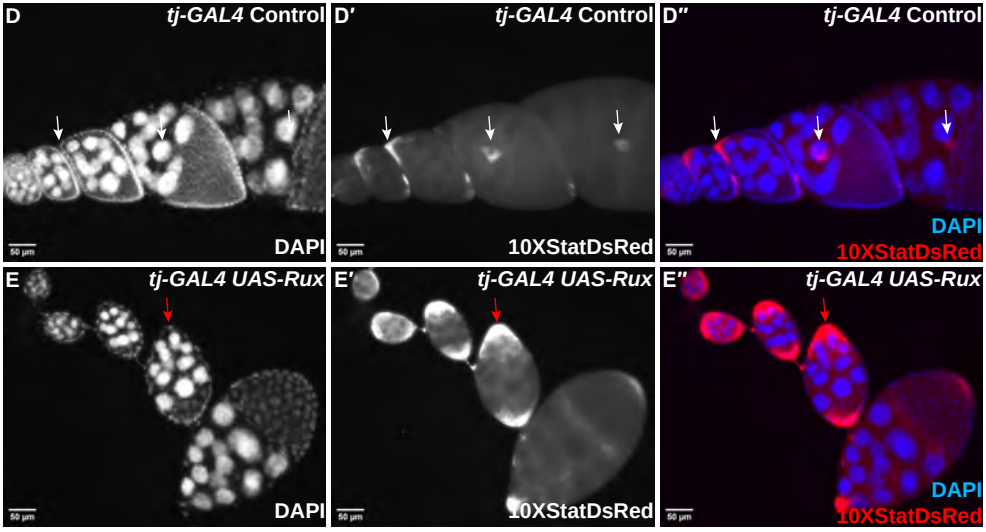
D
tj-GAL4 Control
DAPI
D′
tj-GAL4 Control
10XStatDsRed
D″
tj-GAL4 Control
DAPI
10XStatDsRed
E
tj-GAL4 UAS-Rux
DAPI
E′
tj-GAL4 UAS-Rux
10XStatDsRed
E″
tj-GAL4 UAS-Rux
DAPI
10XStatDsRed

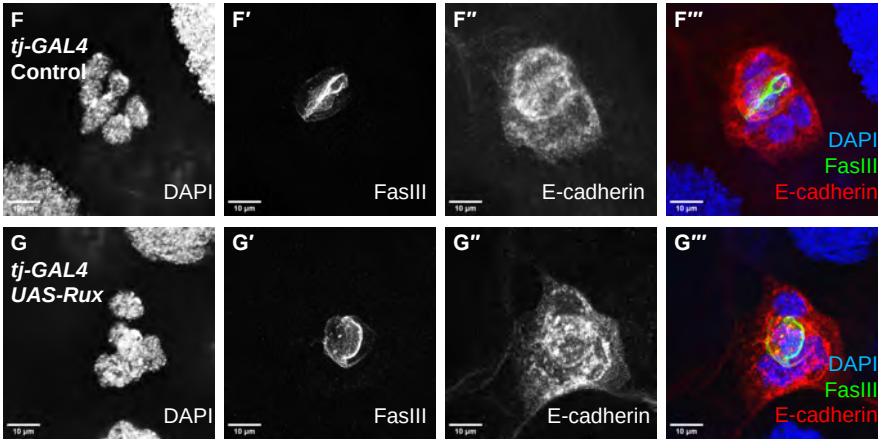
F
tj-GAL4
Control
DAPI
F′
FasIII
F″
E-cadherin
F‴
DAPI
FasIII
E-cadherin
G
tj-GAL4
UAS-Rux
DAPI
G′
FasIII
G″
E-cadherin
G‴
DAPI
FasIII
E-cadherin

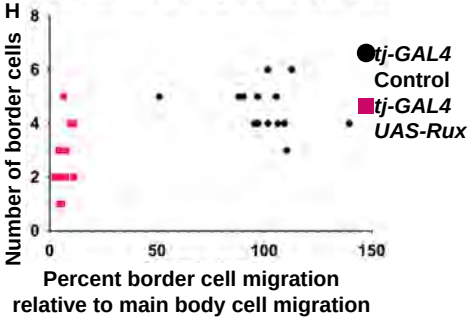
H
Number of border cells
0
2
4
6
8
0
50
100
150
Percent border cell migration
relative to main body cell migration
tj-GAL4
Control
tj-GAL4
UAS-Rux

FIGURE 4

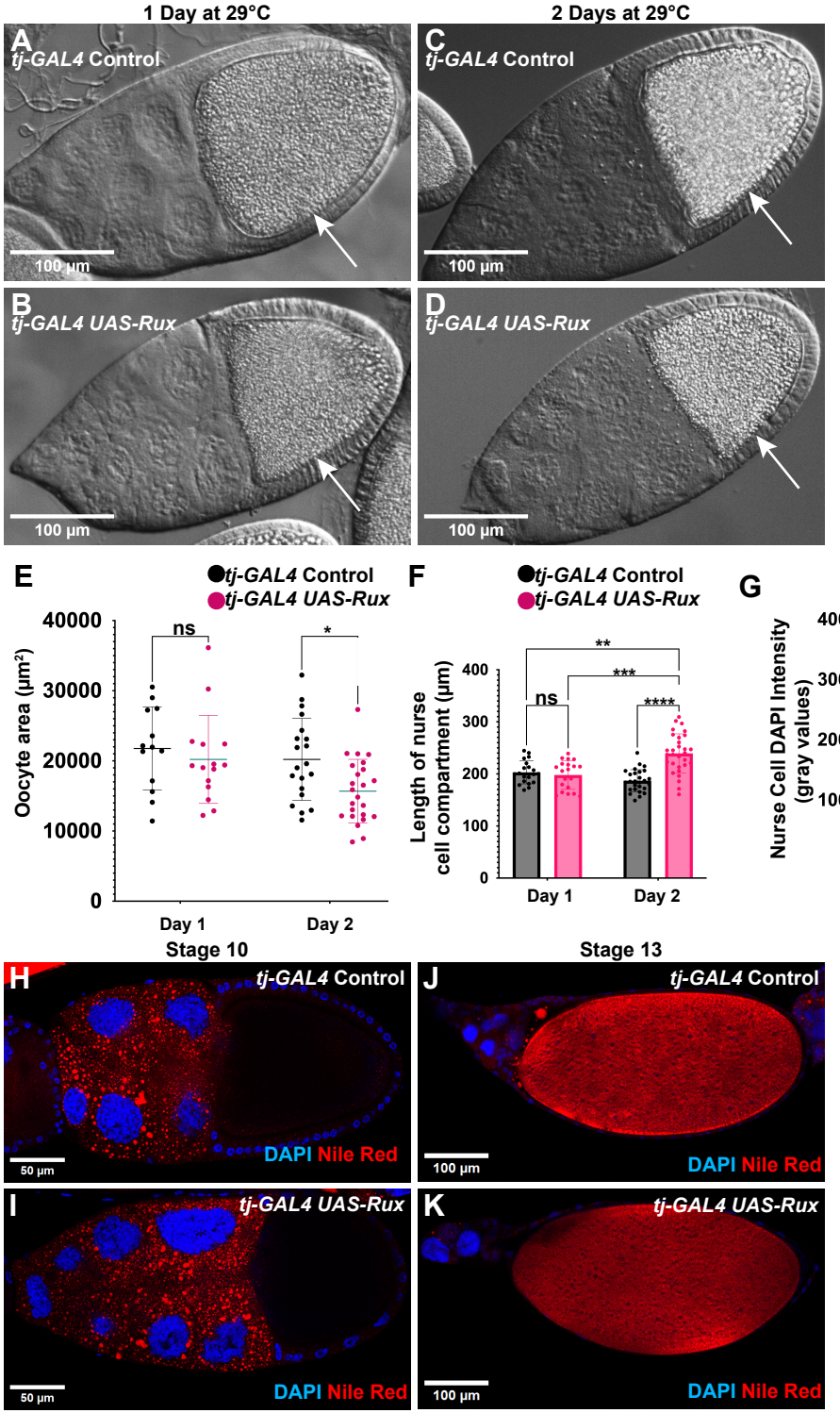
1 Day at 29°C
2 Days at 29°C
A
tj-GAL4 Control
100 µm
C
tj-GAL4 Control
100 µm
B
tj-GAL4 UAS-Rux
100 µm
D
tj-GAL4 UAS-Rux
100 µm
E
tj-GAL4 Control
tj-GAL4 UAS-Rux
Oocyte area (µm²)
40000
30000
20000
10000
0
ns
*
Day 1
Day 2
F
tj-GAL4 Control
tj-GAL4 UAS-Rux
Length of nurse cell compartment (µm)
400
300
200
100
0
ns
**
***
****
Day 1
Day 2
G
Nurse Cell DAPI Intensity (gray values)
4000000
3000000
2000000
1000000
0
ns
+
UAS-Rux
tj-GAL4
Stage 10
Stage 13
H
tj-GAL4 Control
DAPI Nile Red
50 µm
J
tj-GAL4 Control
DAPI Nile Red
100 µm
I
tj-GAL4 UAS-Rux
DAPI Nile Red
50 µm
K
tj-GAL4 UAS-Rux
DAPI Nile Red
100 µm

FIGURE 5

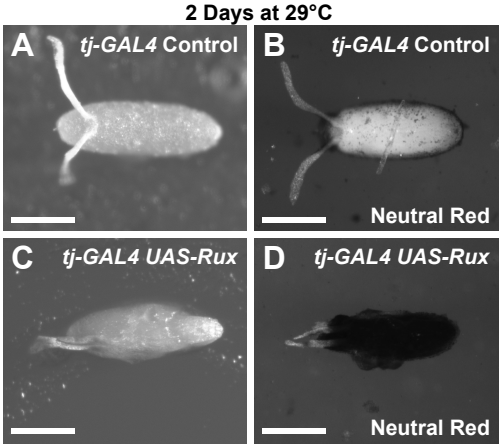
2 Days at 29°C
A
tj-GAL4 Control
B
tj-GAL4 Control
Neutral Red
C
tj-GAL4 UAS-Rux
D
tj-GAL4 UAS-Rux
Neutral Red

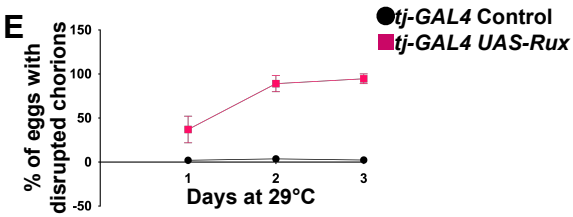
E
tj-GAL4 Control
tj-GAL4 UAS-Rux
% of eggs with disrupted chorions
150
100
50
0
-50
1
2
3
Days at 29°C

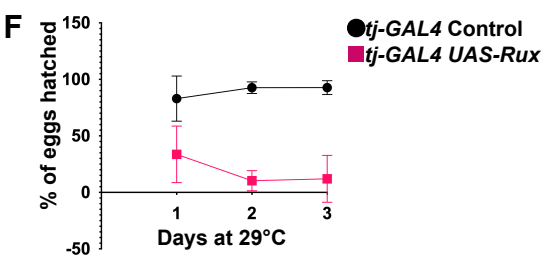
F
tj-GAL4 Control
tj-GAL4 UAS-Rux
% of eggs hatched
150
100
50
0
-50
1
2
3
Days at 29°C

FIGURE 6

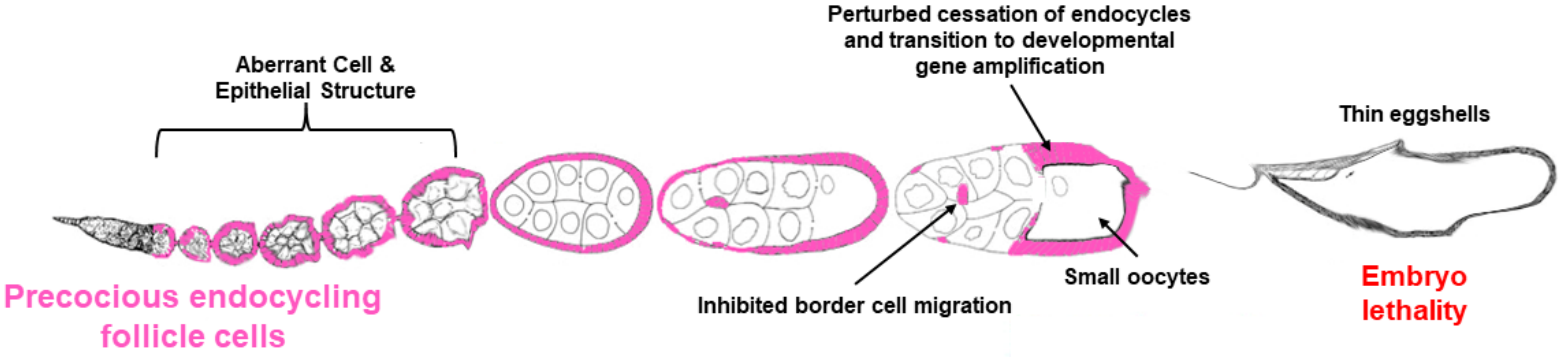
Aberrant Cell &
Epithelial Structure
Perturbed cessation of endocycles
and transition to developmental
gene amplification
Thin eggshells
Precocious endocycling
follicle cells
Inhibited border cell migration
Small oocytes
Embryo
lethality